Deriving dynamical models from paleoclimatic records: application to glacial millennial-scale climate variability

Frank Kwasniok*
School of Engineering, Computing and Mathematics, University of Exeter, North Park Road, Exeter EX4 4QF, United Kingdom

Gerrit Lohmann
Alfred Wegener Institute for Polar and Marine Research, Bussestraße 24, 27570 Bremerhaven, Germany
(Dated: September 17, 2009)

A method for systematically deriving simple nonlinear dynamical models from ice-core data is proposed. It offers a tool to integrate models and theories with paleoclimatic data. The method is based on the unscented Kalman filter, a nonlinear extension of the conventional Kalman filter. Here, we adopt the abstract conceptual model of stochastically driven motion in a potential that allows for two distinctly different states. The parameters of the model, that is, the shape of the potential and the noise level are estimated from a North Greenland ice-core record. For the glacial period from 70 to 20 ky before present, a potential is derived that is asymmetric and almost degenerate. There is a deep well corresponding to a cold stadial state and a very shallow well corresponding to a warm interstadial state.

PACS numbers: 92.70.Aa, 05.45.Tp

I. INTRODUCTION

The subject of past and future abrupt climate changes has been extensively discussed in recent years (e. g., [1]). In particular, one seeks to understand the abrupt climate transitions between cold stadials and warm interstadials during the last glacial period, the so-called Dansgaard-Oeschger (DO) events [2]. Their origin is still controversial; it is not at all obvious which part of the earth's climate system is responsible for abrupt changes. Some attribute them to a temporary collapse and resumption of the Atlantic meridional overturning cell [3]. Other hypotheses refer to internal oscillations of the atmosphere-ocean-cryosphere system [4–7] or external forcing mechanisms [8, 9].

Besides the work with relatively complex numerical models, it was tried to reduce the system to low-order, box, and conceptual models. Often a bistable nonlinear system has been assumed in which shifts between the two distinctly different states are triggered randomly by stochastic forcing [10, 11]. Stochastic resonance [3, 12–14] may or may not play a role in such a model.

Here, we follow a complementary approach in deriving a dynamical model purely from the data. The method is based on unscented Kalman filtering, a nonlinear extension of conventional Kalman filtering. This technique allows to consistently estimate parameters in deterministic and stochastic nonlinear models. Such methodology has been applied successfully in engineering and robotics [15, 16] as well as the nonlinear dynamics community [17, 18] but has not yet been adopted in paleoclimatology. In the present study, we apply this method to determine parameters within the model setting of nonlinear stochastically driven motion in a potential. This model is quite abstract and does not refer to a particular physical mechanism. We focus on the methodology that could also be used for parameter estimation in more physically motivated low-order models.

II. ICE-CORE DATA

The present study is based on the record of δ^{18}O as a proxy for Northern Hemisphere temperatures from the North Greenland Ice Core Project (NGRIP) ice core covering the last 120 ky (1 ky = 1000 years) [19]. When looking at the whole record extending from the present to the last interglacial period the data are heavily nonstationary with switches between interglacial, glacial, and present-day climate. In order to focus on the DO oscillations, we restrict our analysis to the last glacial period. We actually use the record for the time period from 70 to 20 ky before present (Fig. 1). It appears reasonable to assume that the data are stationary for that time span. The mean for that period is -42.13 permille; it is removed from the data set prior to the analysis as the dynamical model is formulated as an anomaly model. The sampling interval of the data is $\delta t = 0.05$ ky resulting in 1000 data points used for the analysis.

The ice-core data are subject to some uncertainties. The instrumental measurement error is very small compared to the variance of the data [19]. However, the interpretation of the δ^{18}O values as temperatures is not one to one; other climatological aspects such as precipitation may also be reflected in the isotope record. Moreover, there might be inaccuracies in the age model due to uneven layers as deeper ice is more compressed.

*Electronic address: F.Kwasniok@exeter.ac.uk

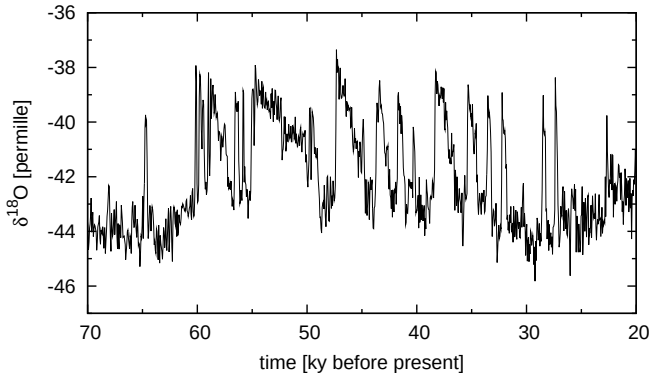

FIG. 1: δ^{18}O record from the NGRIP ice core during the last glacial period.

III. NONLINEARITY IN THE ICE-CORE DATA

In order to assess the level of nonlinearity and make a case for nonlinear modeling of the ice-core data we first perform a test for nonlinearity using the method of surrogate time series. We actually employ a refined procedure [20] which tests against the null hypothesis of a nonlinearly rescaled Gaussian linear stochastic process rather than just a Gaussian linear stochastic process. The generated surrogate time series have both the same power spectrum and the same probability distribution as the original data. This technique yields a stronger test for genuine nonlinear structure (and not just non-Gaussianity) than earlier methods which suffer from higher rates of spurious detection of nonlinearity. As test statistic for measuring nonlinearity we use the mean absolute one-step prediction error of a locally constant (analogue) predictor. The predictor is built in time-delay space of dimension 3, comprising the current observation and the previous two observations; it is based on 50 nearest neighbors with respect to the Euclidian norm. Figure 2a shows the distribution of mean absolute prediction error estimated from 10000 surrogate time series together with the prediction error in the ice-core data. There is very strong evidence for nonlinearity in the ice-core record. The prediction error in the ice-core data is smaller than in any of the surrogates; the null hypothesis can be rejected at any significance level resolved with 10000 realizations. However, the reduction in prediction error compared to the surrogates is relatively moderate (about 8% on the mean of the surrogate distribution). Thus, nonlinear structure and determinism are weak. The ice-core record has a strongly stochastic character; we expect a high dynamical noise level when modeling it.

The surrogate data test for nonlinearity is most reliable for stationary time series; the effect of non-stationarities on the properties of the test is hard to quantify. In order to reduce the mild nonstationarity present in the ice-core data we apply the same nonlinearity test detailed above also to the one-step increment time series rather

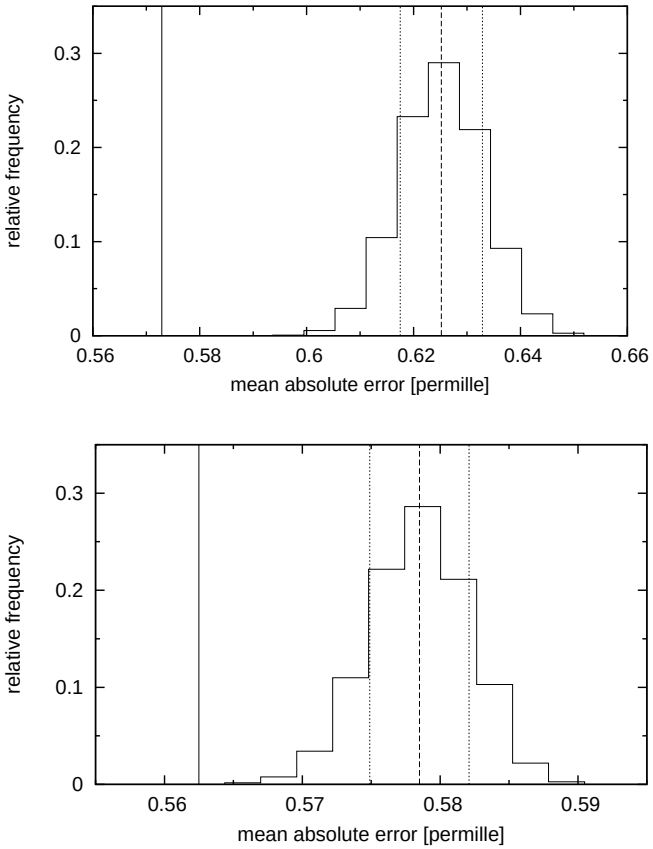

FIG. 2: (a) Distribution of mean absolute prediction error as estimated from 10000 surrogate time series. Dashed vertical line gives the mean value of the distribution; the two dotted vertical lines indicate one standard deviation. Solid vertical line gives the prediction error in the ice-core time series. See text for explanation. (b) As (a), but for the one-step increment time series.

than the ice-core record itself. The results are given in Fig. 2b. Again, nonlinearity can be detected at any significance level resolved with 10000 surrogate time series. The nonlinearity in the increment time series is weaker than in the original record as one expects as the noise level in the increment time series is higher than in the time series itself.

IV. DYNAMICAL MODEL

It has been argued that abrupt paleoclimatic changes might be related to a shift between two distinctly different states in a stochastically driven nonlinear system (e. g., [3, 14]). Similar arguments have been made with regard to possible climate changes in the future. In the present study, we adopt the simple conceptual model of stochastically driven motion in a one-dimensional potential landscape. The dynamics are governed by the

stochastic differential equation

$$\dot{z} = -\frac{dU}{dz} + \sigma\eta. \tag{1}$$

The variable z refers to a mean Northern Hemisphere temperature and is here identified with the isotope record. The deterministic drift is given by a potential that is assumed to be of the form

$$U(z) = a_4 z^4 + a_3 z^3 + a_2 z^2 + a_1 z \tag{2}$$

with free parameters $\{a_i\}_{i=1}^4$ that are to be determined. This ansatz for the potential may be regarded as the simplest model that possibly allows for two distinct stable states separated by a potential barrier. The parameters are readily interpretable: a_4 determines the width of the potential, a_2 influences the height of the potential barrier (if any), whereas a_3 and a_1 control the degree of asymmetry in the location and depth of the two potential wells. η denotes a Gaussian white noise with zero mean and unit variance; σ is the standard deviation of the stochastic forcing.

V. MODEL ESTIMATION FROM DATA

A. The unscented Kalman filter

The unscented Kalman filter (UKF) is a nonlinear extension of the conventional Kalman filter [15]. It offers a flexible and powerful tool for recursive estimation of unobserved states and parameters in nonlinear systems from incomplete, indirect and noisy observations. Unlike the widely used extended Kalman filter, the UKF keeps the full system dynamics rather than linearizing it, leading to a superior treatment of nonlinearities. The UKF truncates the filter probability density to a Gaussian in each iteration by only propagating first and second moments but neglecting higher-order moments. The method is applicable to deterministic as well as stochastic models [17]. Here, the UKF is only briefly described in the form it is actually used in the present context. Readers interested in theoretical and technical issues of the method in more detail are refered to the literature [15–18].

The UKF deals with estimation in nonlinear state space models. A state space model consists of two parts: a dynamical (or state) equation and an observation (or measurement) equation. The dynamical equation is

$$\mathbf{z}_t = \mathbf{f}(\mathbf{z}_{t-1}, \boldsymbol{\lambda}) + \boldsymbol{\eta}_t \tag{3}$$

where $\mathbf{z}$ is a state vector of dimension n_s, $\mathbf{f}$ is a nonlinear function, $\boldsymbol{\lambda}$ is a vector of parameters of dimension n_p and $\boldsymbol{\eta}$ is a Gaussian white noise with zero mean and covariance matrix $\mathbf{Q}$. The observation equation is

$$\mathbf{y}_t = \mathbf{g}(\mathbf{z}_t) + \boldsymbol{\epsilon}_t \tag{4}$$

where $\mathbf{y}$ is a vector of observations of dimension n_o, $\mathbf{g}$ is a (generally) nonlinear observation function and $\boldsymbol{\epsilon}$ is a Gaussian white observational noise with zero mean and covariance matrix $\mathbf{R}$. The UKF addresses the problem of simultaneously estimating the unobserved states $\{\mathbf{z}_t\}_{t=1}^N$ and the parameters $\boldsymbol{\lambda}$ given only time series of the noisy observations $\{\mathbf{y}_t\}_{t=1}^N$. For this purpose, an augmented state vector $\mathbf{x}$ of dimension $n = n_\mathrm{s} + n_\mathrm{p}$ is formed by merging the state vector $\mathbf{z}$ and the parameters $\boldsymbol{\lambda}$; its dynamical evolution is described by an augmented function $\mathbf{f}^\mathrm{a}$ given by eq. (3) augmented by a constant dynamics for the parameters:

$$\begin{aligned}\mathbf{x}_t &= \begin{pmatrix}\mathbf{z}_t \\ \boldsymbol{\lambda}_t\end{pmatrix} = \begin{pmatrix}\mathbf{f}(\mathbf{z}_{t-1}, \boldsymbol{\lambda}_{t-1}) \\ \boldsymbol{\lambda}_{t-1}\end{pmatrix} + \begin{pmatrix}\boldsymbol{\eta}_t \\ \mathbf{0}_{n_\mathrm{p}}\end{pmatrix} \\ &= \mathbf{f}^\mathrm{a}(\mathbf{x}_{t-1}) + \begin{pmatrix}\boldsymbol{\eta}_t \\ \mathbf{0}_{n_\mathrm{p}}\end{pmatrix}\end{aligned} \tag{5}$$

The dynamical noise has augmented covariance matrix

$$\mathbf{Q}^\mathrm{a} = \begin{pmatrix}\mathbf{Q} & \mathbf{0}_{n_\mathrm{s}\times n_\mathrm{p}} \\ \mathbf{0}_{n_\mathrm{p}\times n_\mathrm{s}} & \mathbf{0}_{n_\mathrm{p}\times n_\mathrm{p}}\end{pmatrix}. \tag{6}$$

For the model considered here, the state is only one-dimensional ($n_\mathrm{s} = 1$), the parameters are $\boldsymbol{\lambda} = (a_1, a_2, a_3, a_4)^\mathrm{T}$ ($n_\mathrm{p} = 4$) and the dynamical equation is given by a discretization of eq. (1) using the Euler scheme with step size h:

$$\begin{aligned}z_t &= f(z_{t-1}, a_1, a_2, a_3, a_4) \\ &= z_{t-1} - h(4a_4 z_{t-1}^3 + 3a_3 z_{t-1}^2 + 2a_2 z_{t-1} + a_1) \\ &\quad + \sqrt{h}\,\sigma\eta_t\end{aligned} \tag{7}$$

The variance of the dynamical noise in the discretized system is $Q = h\sigma^2$. The dimension of augmented state space is $n = 5$. We have a single observational time series ($n_\mathrm{o} = 1$) that is simply related to the state by the identity observation function:

$$y_t = z_t + \epsilon_t \tag{8}$$

The UKF then takes a particularly simple form.

Let $\hat{\mathbf{x}}_{t-1|t-1}$ be the estimate of the augmented state vector and $\mathbf{P}^{xx}_{t-1|t-1}$ its covariance matrix at time $t-1$ having processed all data up to time $t-1$. The filter density is represented by a small number of test points, so-called sigma points, that are propagated through the nonlinear dynamical equation. The sigma points have to be chosen carefully in order to ensure that they capture the first and second moments of the transformed density to some order of accuracy [16]. We employ $2n$ sigma points, $\{\mathbf{x}^i_{t-1|t-1}\}_{i=1}^{2n}$, each in augmented state space of dimension n, given as $\left\{\hat{\mathbf{x}}_{t-1|t-1} + \mathbf{v}^j, \hat{\mathbf{x}}_{t-1|t-1} - \mathbf{v}^j\right\}_{j=1}^n$. The vectors $\left\{\mathbf{v}^j\right\}_{j=1}^n$ are the columns of $\mathbf{A}$ where $\mathbf{A}$ can be any matrix satisfying $\mathbf{A}\mathbf{A}^\mathrm{T} = n\mathbf{P}^{xx}_{t-1|t-1}$. Here we calculate $\mathbf{A}$ using the Cholesky decomposition of $\mathbf{P}^{xx}_{t-1|t-1}$. The sigma points are propagated through the dynamical equation and the observation function is applied:

$$\mathbf{x}^i_{t|t-1} = \mathbf{f}^\mathrm{a}\left(\mathbf{x}^i_{t-1|t-1}\right) \tag{9}$$

$$y^i_{t|t-1} = z^i_{t|t-1} \tag{10}$$

The means of the transformed sigma points are

$$\hat{\mathbf{x}}_{t|t-1} = \frac{1}{2n}\sum_{i=1}^{2n}\mathbf{x}^i_{t|t-1} \tag{11}$$

$$\hat{y}_{t|t-1} = \frac{1}{2n}\sum_{i=1}^{2n}y^i_{t|t-1}; \tag{12}$$

the covariances are

$$\mathbf{P}^{xx}_{t|t-1} = \frac{1}{2n}\sum_{i=1}^{2n}\left(\mathbf{x}^i_{t|t-1}-\hat{\mathbf{x}}_{t|t-1}\right)\left(\mathbf{x}^i_{t|t-1}-\hat{\mathbf{x}}_{t|t-1}\right)^{\mathrm{T}} + \mathbf{Q}^{\mathrm{a}} \tag{13}$$

$$\mathbf{P}^{xy}_{t|t-1} = \frac{1}{2n}\sum_{i=1}^{2n}\left(\mathbf{x}^i_{t|t-1}-\hat{\mathbf{x}}_{t|t-1}\right)\left(y^i_{t|t-1}-\hat{y}_{t|t-1}\right) + \mathbf{q}^{\mathrm{a}} \tag{14}$$

$$P^{yy}_{t|t-1} = \frac{1}{2n}\sum_{i=1}^{2n}\left(y^i_{t|t-1}-\hat{y}_{t|t-1}\right)^2 + Q^{\mathrm{a}}_{11} + R \tag{15}$$

with $\mathbf{q}^{\mathrm{a}} = (Q^{\mathrm{a}}_{11},0,0,0,0)^{\mathrm{T}}$. The augmented covariance matrix of the dynamical noise $\mathbf{Q}^{\mathrm{a}}$ is zero except for the element Q^{a}_{11} related to the state variable z which is given by $Q^{\mathrm{a}}_{11} = Q = h\sigma^2$. When reaching a new data point y_t the estimates of the state and the parameters as well as their uncertainties are corrected using the new observation according to the ordinary Kalman update equations

$$\hat{\mathbf{x}}_{t|t} = \hat{\mathbf{x}}_{t|t-1} + \mathbf{K}_t(y_t - \hat{y}_{t|t-1}) \tag{16}$$

$$\mathbf{P}^{xx}_{t|t} = \mathbf{P}^{xx}_{t|t-1} - \mathbf{K}_t P^{yy}_{t|t-1}\mathbf{K}_t^{\mathrm{T}} \tag{17}$$

where $\mathbf{K}_t$ is the Kalman gain matrix given as

$$\mathbf{K}_t = \mathbf{P}^{xy}_{t|t-1}(P^{yy}_{t|t-1})^{-1}. \tag{18}$$

Since the dynamical model is specified here as a continuous-time equation rather than a discrete system the step size h usually has to be taken much smaller than the sampling interval of the data δt. Hence one has to propagate sigma points many times before reaching the next data point and updating according to eqs. (16)–(18).

Note that the algorithm is deterministic even for a stochastic model. It propagates only probability densities and does not refer to individual noise realizations; for a particular observational time series $\{y_t\}_{t=1}^N$ and given initial guesses for the state and the parameters $\hat{\mathbf{x}}_{1|1}$ as well as their uncertainties $\mathbf{P}^{xx}_{1|1}$ the outcome is determined.

Along with the estimates for the state and the parameters the algorithm provides information on their uncertainties. Assuming Gaussian estimation errors, a symmetric 95%-confidence interval for a particular element of the augmented state vector x_i is given as $[\hat{x}_i - 1.96\sqrt{P^{xx}_{ii}}, \hat{x}_i + 1.96\sqrt{P^{xx}_{ii}}]$.

For vanishing observational noise ($R = 0$), the state estimate degenerates to $\hat{z}_{t|t} = y_t$; but parameter estimation is then still useful. For technical reasons, even with no observational noise R is not set eactly to zero but to a very small number, say, $R = 10^{-12}$. This prevents the matrix $\mathbf{P}^{xx}_{t|t}$ from becoming negative definite due to rounding errors when the algorithm proceeds which would cause the Cholesky decomposition to break down.

B. Estimation of the noise level

Besides the parameters $\{a_i\}_{i=1}^4$ one wishes to estimate the noise level σ directly from the data since it is as essential in determining the dynamical behavior of the system as the shape of the potential. Unfortunately, the noise level (both the dynamical and the observational) cannot be systematically estimated within the UKF; it has to be given beforehand based on prior knowledge about the system and the observation process. This is a fundamental weakness of all types of Kalman filters. We propose an adhoc solution to the problem that proves adequate at least for the specific model setting considered here. Assuming the observational noise level to be known, the dynamical noise level is determined by fitting some global statistical quantity that characterizes the long-term dynamics of the system. Stochastically driven motion in a bistable potential is characterized by a stationary probability density that is peaked around the minima of the potential. The sharpness of the probability density depends crucially on the noise level. Therefore it appears reasonable that for an adequate model the stationary probability density $p_{\mathrm{m}}(z)$, or in the case of observational noise the observed probability density $p^{\mathrm{o}}_{\mathrm{m}}(y)$, should match the empirical density of the data. For this purpose, we run the UKF for different noise levels and monitor the deviation between the observed cumulative distribution function of the model $\Phi^{\mathrm{o}}_{\mathrm{m}}$ and that of the data Φ_{d} defined as the Kolmogorov-Smirnov distance

$$D = \max_y |\Phi^{\mathrm{o}}_{\mathrm{m}}(y) - \Phi_{\mathrm{d}}(y)| \tag{19}$$

as a function of the noise level and search for a minimum. For the model considered here, it is known that

$$p_{\mathrm{m}}(z) \sim \exp\left[-2U(z)/\sigma^2\right] \tag{20}$$

with a proper normalization constant [21]. The normalization and the cumulative distribution can be obtained by numerical integration. In the case of observational noise, the probability density of the observed variable y is given by the convolution integral

$$p^{\mathrm{o}}_{\mathrm{m}}(y) \sim \int_{-\infty}^{+\infty} p_{\mathrm{m}}(z)\exp\left[-\frac{(y-z)^2}{2R}\right]dz \tag{21}$$

which is solved and normalization and the cumulative distribution are found numerically. The distribution function of the data is given empirically as $\Phi_{\mathrm{d}}(y) = N_y/N$ where N_y is the number of data points less or equal y and N is the size of the whole data set.

In general, for dynamical systems that are not so much characterized by the shape of their stationary density

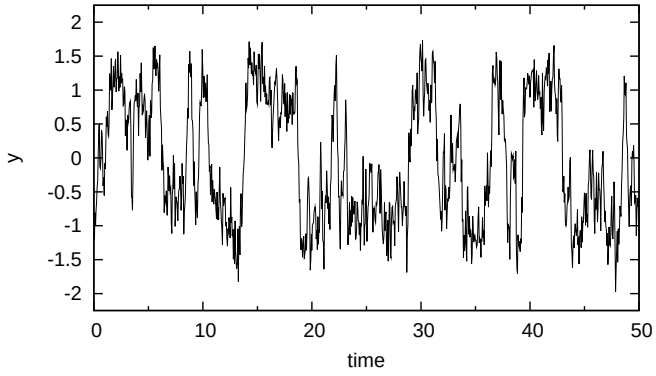

FIG. 3: Sample trajectory of stochastically driven motion in a symmetric double-well potential with observational noise.

other criteria rather than the measure D may be more appropriate to determine the noise level. Possible alternatives are moment-matching conditions (e. g., tuning the mean or the variance of some important quantity in the system) as well as fitting a characteristic timescale of the system given by the autocorrelation function at some meaningful lag, the decorrelation time or a regime transition time.

VI. DEMONSTRATION OF THE METHOD ON SIMULATED DATA

In order to assess and demonstrate the ability of the UKF to reliably identify parameters and noise strengths in the model setting considered here we first apply it to simulated data. We assume a symmetric double-well potential given by $U(z) = z^4 - 2z^2$, that is, $(a_1, a_2, a_3, a_4) = (0, -2, 0, 1)$; the noise level is $\sigma = 1.5$. The system is simulated for 1000 time units using the Euler scheme with a step size of 10^{-5}; the sampling interval is $\delta t = 0.05$. Figure 3 shows a sample trajectory of the system. The time series is contaminated with observational noise of standard deviation 0.1. The Kramers mean waiting time for a transition from one stable state to the other [21] is about 2.7 which when interpreted as ky is about the same as in the ice-core data [11]. The symmetry of the potential is not fixed when applying the UKF algorithm; all four parameters $\{a_i\}_{i=1}^4$ are treated as unknown and are to be estimated. The UKF is initialized with $(a_1, a_2, a_3, a_4) = (2, 2, 2, 2)$ which is quite far away from the true solution. The initial state estimate is given by the first observation: $\hat{z}_{1|1} = y_1$. The initial uncertainties are set to 1 for all four parameters; the initial state uncertainty is 0.01 in accordance with the observational noise level. The step size in the UKF is $h = \delta t/100 = 0.0005$; we set $R = 0.01$.

The UKF is run for different noise levels and the actual noise level is determined as described above. By matching the distribution functions of the model and the data sample the noise level is correctly identified as $\sigma = 1.5$ (Fig. 4a). Without observational noise the minimum of D at 1.5 is even sharper (not shown). Figures 4b and 4c give the estimated parameter values together with 95%-confidence intervals as the algorithm proceeds through the time series. The final values at $t = 1000$ are: $a_4 = 1.01 \pm 0.06$, $a_3 = 0.03 \pm 0.06$, $a_2 = -2.01 \pm 0.15$ and $a_1 = -0.05 \pm 0.17$. The estimates are very accurate; for all parameters, the true values lie well within the confidence intervals. The reconstructed potential is extremely close to the true one (Fig. 4d). We conclude that the UKF together with the heuristic estimation of the noise level is capable of accurately estimating parameters for Brownian motion in a potential landscape even if the time series is corrupted by observational noise.

VII. RESULTS FOR THE ICE-CORE DATA AND DISCUSSION

The ice-core record was processed in the same way as the simulated data. The initial guess for the potential was taken to be $U(z) = z^4 - 2z^2$, that is, $(a_1, a_2, a_3, a_4) = (0, -2, 0, 1)$ with unit uncertainties. The initial estimate of the state z was taken as the first data point. The measurement error of the ice-core data is indicated to be as small as 0.07% [19]. This suggests a value of about $R = 0.001$ for the variance of the observational error. Actually, when setting $R = 10^{-12}$ the results are virtually indistinguishable from those obtained with $R = 0.001$. Observational noise is negligable for the present ice-core data compared to the dynamical noise that is of order unity. We therefore adopt the value $R = 10^{-12}$ and the dynamical variable z can be identified with the observed variable y. The step size in the UKF algorithm was set to $h = \delta t/100 = 0.0005$ ky. The data set spanning a period of 50 ky with 1000 observations turned out to be too short to obtain well-converged estimates for the parameters with small confidence intervals. Therefore the data were processed ten times in order to improve the estimates. Each new sweep was started with the final estimates for the parameters and uncertainties from the preceeding sweep; however, the off-diagonal elements of $\mathbf{P}^{xx}$ were set to zero [17].

For the ice-core data, the parameter estimation turns out to be ill-conditioned with respect to the parameter a_1. The estimate for a_1 is still drifting and has large uncertainty after processing the data ten times. This is due to the almost degenerate shape of the potential and the high dynamical noise level (see below). It does not occur with the simulated data above as the potential there has a distinct shape with two deep wells and the noise level is smaller. The problem is removed by imposing a moment-matching condition as a constraint on the parameters. It appears reasonable to require that the model has the same mean state as the ice-core data, that

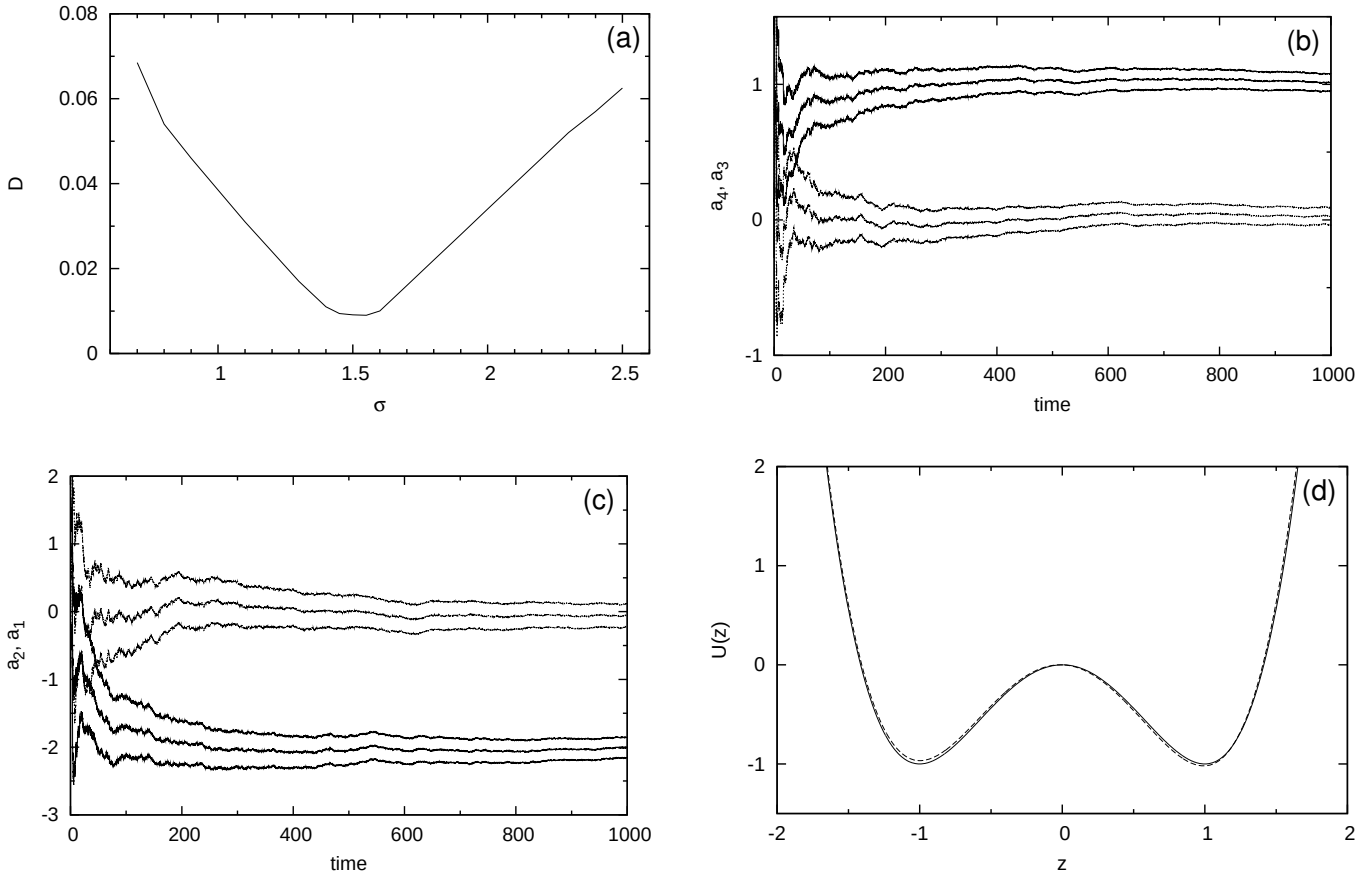

FIG. 4: Simulated data: (a) Estimation of noise level: Kolmogorov-Smirnov distance between the probability distributions of the model and the data as a function of the noise level. (b) Estimates for a_4 (solid) and a_3 (dotted) together with 95%-confidence intervals as a function of time. (c) Estimates for a_2 (solid) and a_1 (dotted) together with 95%-confidence intervals as a function of time. (d) True (solid) and reconstructed (dashed) potential.

is, $\langle z\rangle = \int_{-\infty}^{+\infty} z\, p_{\rm m}(z)\, dz = 0$, leading to the condition

$$\int_{-\infty}^{+\infty} z \exp\left[-2U(z)/\sigma^2\right] dz = 0. \qquad (22)$$

It is straightforward to verify that for fixed parameters a_4, a_3, a_2 and noise level σ the mean state $\langle z\rangle$ tends to $+\infty$ as a_1 goes to $-\infty$, tends to $-\infty$ as a_1 goes to $+\infty$ and has a monotonic dependence on a_1 in between. Thus eq. (22) uniquely determines a_1 for given a_4, a_3, a_2 and σ. The integral in eq. (22) is evaluated numerically; the root is then found by running 15 iterations of the bisection algorithm starting with the (conservative) interval $[-10, 10]$ for a_1. The UKF is modified in that only a_4, a_3 and a_2 are parameters to be determined. We then have $n_{\rm p} = 3$ and $n = 4$. a_1 is treated as a constant in the UKF and updated according to eq. (22) at each data point after the Kalman update using the current estimates for a_4, a_3 and a_2. Eq. (22) is still valid in the case of observational noise with mean zero as such a noise does not alter the mean state of the system ($\langle y\rangle = \langle z\rangle$).

The UKF was run for different levels of dynamical noise and the model probability distribution function monitored and compared to that of the data. Here, the measure D turns out to be inconclusive (Fig. 5a). There is a minimum at 3.2 but the values of D on the whole interval between 3.2 and 4.2 are quite similar given that the probability distribution of the data is estimated from only 1000 data points. Therefore the estimate for the noise level is backed up by looking at other quantities. Figure 5b displays the standard deviation of z in the model as a function of the noise level. It increases almost linearly over the interval between 2.2 and 5.1 and there is a sharp match with the data at $\sigma = 3.8$. In Fig. 5c, the autocorrelation function at lag 1, that is, at $\delta t = 0.05$ ky as a function of the noise level is given. The estimates are calculated from an integration of the model for 5000 ky (100000 data points); some sampling fluctuations are still visible. The autocorrelation decreases more or less linearly with the noise level; the autocorrelation of the data is matched at $\sigma = 3.7$. Taking both standard deviation and autocorrelation into account, we adopt $\sigma = 3.75$ as the dynamical noise level of the potential model. In Figs. 5d and 5e, the estimates of the parameters are displayed as a function of time together with 95%-confidence intervals. There are inhomogenieties after about 10 ky of each sweep corresponding to the visible

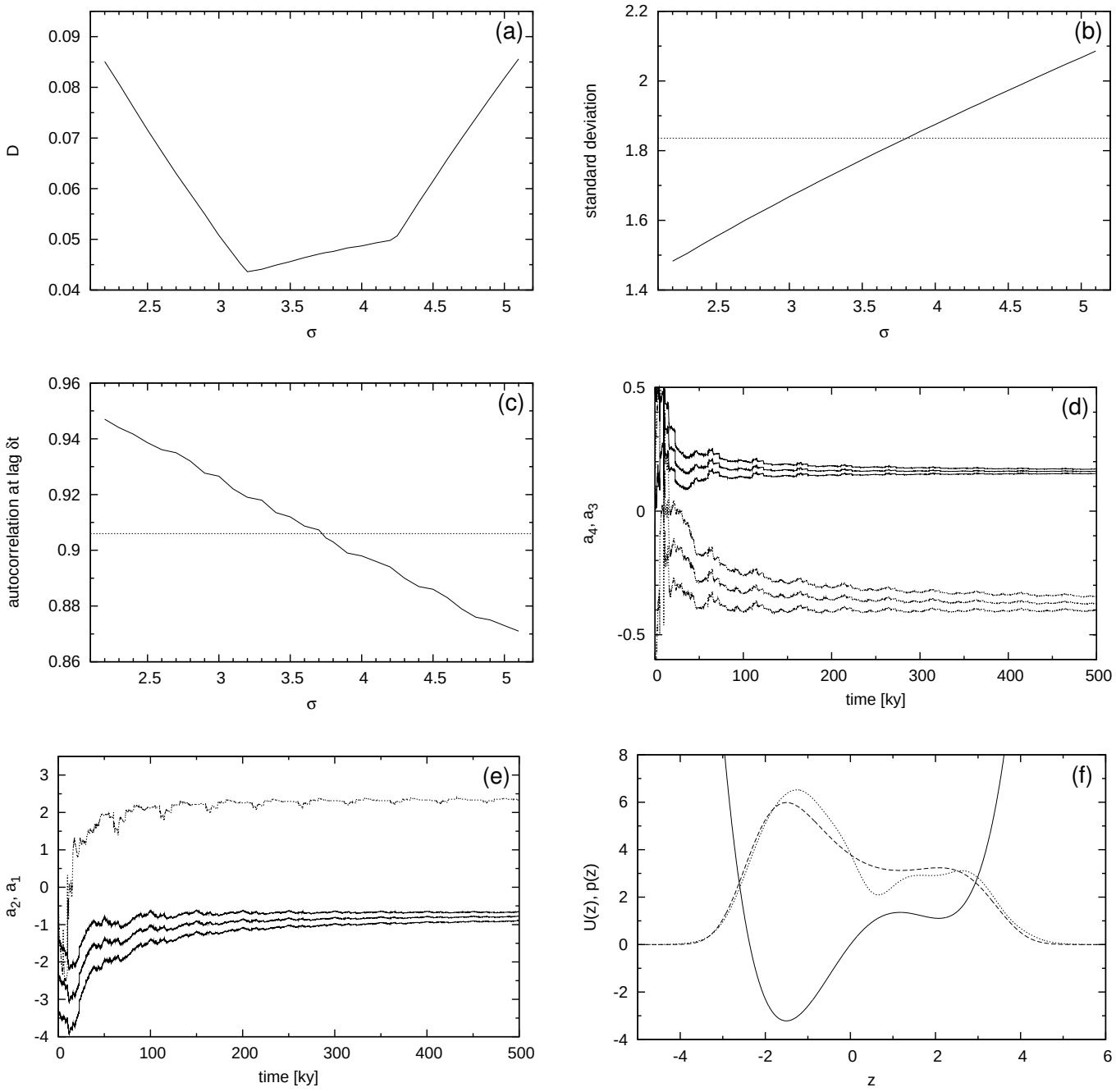

FIG. 5: Ice-core data: (a) Estimation of noise level: Kolmogorov-Smirnov distance between the probability distributions of the model and the data as a function of the noise level. (b) Standard deviation of z in the model as a function of the noise level (solid). Dotted horizontal line indicates the standard deviation of the data. (c) Autocorrelation at lag δt in the model as a function of the noise level (solid). Dotted horizontal line indicated the autocorrelation at lag δt in the data. (d) Estimates for a_4 (solid) and a_3 (dotted) together with 95%-confidence intervals as a function of time. (e) Estimates for a_2 together with 95%-confidence intervals (solid) and a_1 (dotted) as a function of time. (f) Potential derived from the data (solid) together with probability densities of the model (dashed) and the data (dotted).

inhomogeniety in the ice-core record at about 60 ky before present (Fig. 1). After ten sweeps well-converged estimates for all parameters with reasonably small confidence intervals are obtained. Taking averages over the last sweep of 50 ky, the values of the parameters are: $a_4 = 0.16 \pm 0.01$, $a_3 = -0.37 \pm 0.03$, $a_2 = -0.79 \pm 0.12$, and $a_1 = 2.34$. The potential is highly asymmetric and almost degenerate (that is, close to a bifurcation); there is a deep well corresponding to a cold stadial state and a very shallow well corresponding to a warm interstadial state (Fig. 5f). The finding that the system is right at the bifurcation to multiple equilibria might help under-

stand the large and abrupt millennial-scale climate fluctuations during the last glacial, associated with the DO oscillations and Heinrich/DO tandems [22]. The stationary probability density of the model and the probability density of the ice-core data are plotted together with the potential (Fig. 4f). The probability density of the data is calculated using a standard Gaussian kernel estimator. Both probability densities are normalized to 25 in order to increase the readability of the plot. The model captures the two maxima in the probability density corresponding to the stadial and interstadial state with approximately the correct population; there is a slight shift in the amplitudes of the states themselves on the z-axis. The mean and standard deviation of z in the model are $\mu = 0$ and $s = 1.83$ compared to $\mu = 0$ and $s = 1.84$ in the ice-core data.

In Fig. 6, the autocorrelation function of the potential model is contrasted with the sample autocorrelation function of the ice-core data. Moreover, the autocorrelation functions of an AR(1) model and an AR(3) model (the linear model with the same number of parameters as the nonlinear model) are given for comparison. The potential model captures the initial decay of the autocorrelation very well but then decays too fast at larger lags. However, the memory at larger lags in the autocorrelation function of the ice-core data turns out to be more an artefact due to the nonstationarity of the data rather than genuine long-term memory due to a deterministic dynamical mechanism. This is revealed by looking at autocorrelation functions over parts of the time series where the data is more stationary (not shown). The memory at larger lags is then greatly reduced and the autocorrelation function is much closer to that of the potential model. The model is stationary by construction and can only model the stationary part of the autocorrelations. The nonlinear potential model outperformes the AR(1) model, albeit not dramatically, and its autocorrelation function is virtually indistinguishable from that of the AR(3) model. The nonlinear potential model captures the linear properties of the data as well as the linear model of the same complexity. On top of this, it models some nonlinear features such as the strongly non-Gaussian probability density whereas the probability density of an AR model is always Gaussian.

In Figure 7, a sample trajectory of the model derived from the ice-core data is displayed. The stochastic equation was integrated using the Euler scheme with step size 10^{-5} and sampled with $\delta t = 0.05$. The ice-core time series is shown again, here with its mean value removed, to facilitate comparison. The trajectory bears clear similarity with the ice-core record; transitions from the cold stadial state to the warm interstadial state and back are reproduced on the correct timescale. However, the model is not able to capture the pronounced temporal asymmetry of DO events. DO events are systematically characterized by an abrupt warming followed by a slow cooling which is not the case in the model.

The ansatz of eq. (2) can be generalized to $U(z) = \sum_{i=1}^{L} a_i z^i$ with L being an even integer. For the data set considered here, it was found that using a sixth-order polynomial instead of a fourth-order polynomial only provides a slightly better capture of the stationary density but does not visibly improve the dynamical behavior of the model. A higher-order potential is useful if the data display more than two distinctly different states.

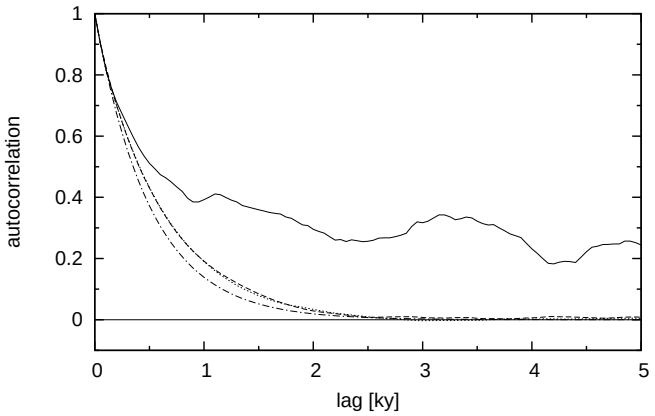

FIG. 6: Sample autocorrelation function of the ice-core data (solid) and autocorrelation functions of the nonlinear potential model (dashed), an AR(1) model (dot-dashed) and an AR(3) model (dotted).

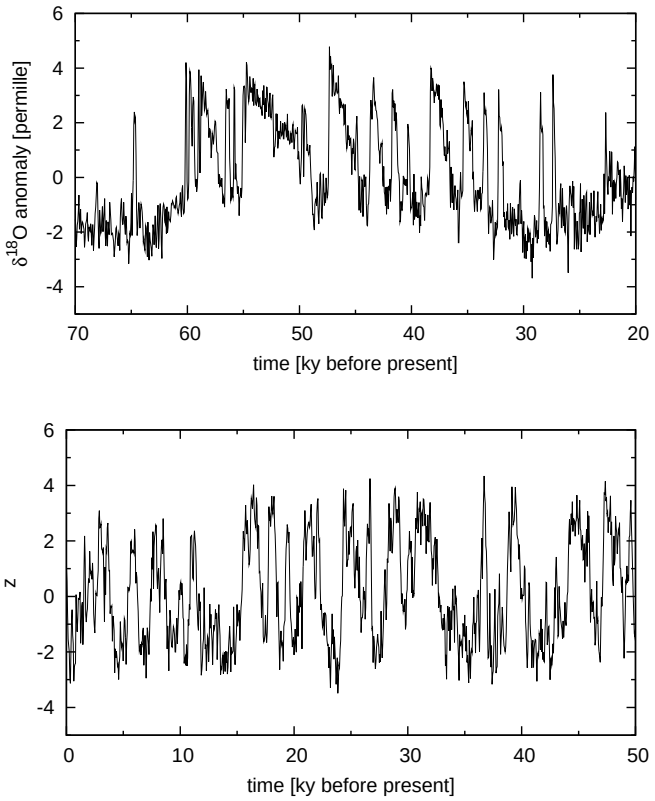

FIG. 7: (a) δ^{18}O record from the NGRIP ice core during the last glacial period with the mean value removed. (b) Sample trajectory of the model derived from the ice-core data.

VIII. ALTERNATIVE METHOD

Given that observational error is negligable in the present ice-core data the one-to-one correspondence of the stationary density to the potential [eq. (20)] suggests deriving the potential directly from the probability density of the data (cf., [10]). Eq. (20) yields

$$U = -\frac{\sigma^2}{2} \log p_{\mathrm{d}} \tag{23}$$

where p_{d} is the probability density of the data. A least-squares fit of the ansatz of eq. (2) to $-\log p_{\mathrm{d}}$ provides the shape of the potential that is independent of the noise level up to a constant factor. The stationary density of the corresponding model and all its moments are independent of the noise level. The timescale of the system remains undetermined, suggesting a fit to the autocorrelation of the data to obtain the noise level. Actually, a weighted least-squares procedure was used, weighing each data point with the probability density of the data at that point. This guarantees the closest fit in regions where the data are. A standard least-squares algorithm overweighs the outside regions of the potential at the expense of the inner region around zero that is indeed most interesting. The noise level is determined by fitting the autocorrelation at lag δt to that of the data. Again, the autocorrelation decreases monotonically with increasing noise level (not shown). A match is obtained for $\sigma = 3.75$, just the same value adopted before. The potential for that noise level is shown in Fig. 7 together with the probability density of the corresponding model and the data, allowing a direct comparison with the UKF result (Fig. 4f). The coefficients of the potential are $a_4 = 0.15$, $a_3 = -0.44$, $a_2 = -0.65$ and $a_1 = 2.89$. The two potentials are fairly similar. The Kolmogorov-Smirnov distance between the probability distributions of the model and the data is here $D = 0.034$, somewhat smaller than for the UKF model. The mean and standard deviation of z in the model are $\mu = 0$ and $s = 1.87$, a slight overestimation of the variance of the system. The autocorrelation function is very close to that for the UKF model (not shown), the UKF model being slightly closer to the autocorrelation of the data. It was found that using a sixth-order polynomial for the potential instead of a fourth-order one does not provide a significant improvement of the model performance in any of the quantities mentioned above.

In the present model setting, the simple least-squares fitting method already yields similar results to the more elaborated UKF method. The system is already very much characterized by its stationary density alone. It should be noted, however, that the least-squares fit to the probability density is very limited whereas the UKF approach is much more general. Already with observational noise, the least-squares fit is no longer possible (cf., [24]). Moreover, most dynamical systems do not have a straight correspondence between the equation of motion and the stationary density such as eq. (20) at all. They are not uniquely identifiable from only the stationary density.

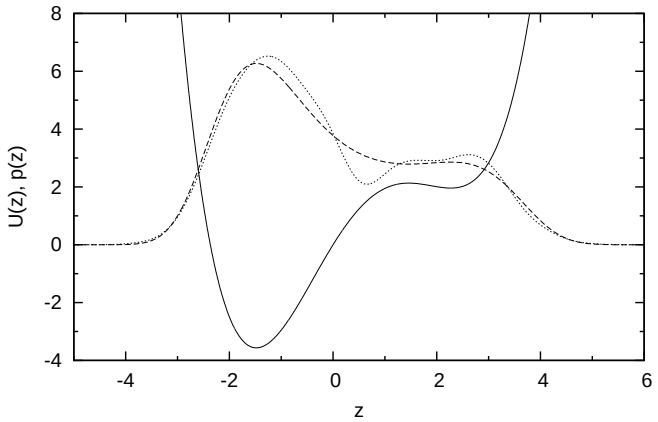

FIG. 8: Potential derived by least-squares fit from the probability density of the ice-core data (solid) together with probability densities of the model (dashed) and the data (dotted).

IX. CONCLUSIONS AND OUTLOOK

We have introduced and verified a methodology for deriving dynamical models from paleoclimatic time series. As an example, we have obtained a stochastically driven nonlinear potential model from NGRIP ice-core data. It is able to capture some basic statistical properties of the data. Admittedly, the model does not provide a physical mechanism and thus conclusions about the underlying dynamics are somewhat limited. Our analysis reveals that the system switches randomly between two different states and that the climate state may linger for a longer time around the locally extreme points of the potential. On the other hand, the abstract character of our model might be regarded as an advantage in that it is based purely on data. The question of the underlying dynamics is related to the stability of the stadial and interstadial states. The present method may be used to perform a bifurcation analysis of a paleoclimatic time series by tracing changes in the shape of the potential, the number of states and their stability over time [23].

The model derived here could be used as a null-hypothesis for DO-like oscillations against which other models should be tested. This constitutes a stronger test than the common null-hypotheses of white or red noise [26].

A possible extension of the present work lies in adding a deterministic periodic forcing to eq. (1), that is, a periodic variation of the parameter a_1 in the potential in order to investigate the importance of stochastic resonance (cf., [11]). Another interesting point would be the inclusion of multiplicative (that is, state-dependent) noise and its influence on the performance of the model. There has indeed been evidence that the statistical properties of the data are different in the stadial and the interstadial state [25, 26]. Other extensions refer to colored or heavy-tailed noises.

The methodology employed in the present paper is fairly general and applicable to a variety of different de-

terministic and stochastic low-order models. It has also been used to derive a nonlinear stochastically driven oscillator model from the ice-core data [24]. It could serve as a tool to compare the different conceptual models that have been proposed to explain the dynamics of DO events and to clarify to what extent they are quantitatively in accordance with paleoclimatic data records.

Acknowledgments

The authors would like to thank H. U. Voss for clarifying discussions on the methodology of unscented Kalman filtering. Thanks go to the NGRIP community for making the data available to us. This work was partly funded by the Bundesministerium für Bildung und Forschung through DEKLIM and MARCOPOLI, and by the Deutsche Forschungsgemeinschaft through DFG Research Centre Ocean Margins at the University of Bremen.

[1] R. B. Alley and 10 coauthors, Science **299**, 2005 (2003).
[2] W. Dansgaard and 10 coauthors, Nature **364**, 218 (1993).
[3] A. Ganopolski and S. Rahmstorf, Phys. Rev. Lett. **88**, 038501 (2002).
[4] M. Winton, in *Ice in the Climate System*, edited by W. R. Peltier (Springer, Berlin, 1993), pp. 417–432.
[5] K. Sakai and W. R. Peltier, J. Climate **10**, 949 (1997).
[6] M. Schulz, A. Paul, and A. Timmermann, Geophys. Res. Lett. **29**, 2193 (2002).
[7] A. Timmermann, H. Gildor, M. Schulz, and E. Tziperman, J. Climate **16**, 2569 (2003).
[8] A. Ganopolski and S. Rahmstorf, Nature **409**, 153 (2001).
[9] H. Braun, M. Christl, S. Rahmstorf, A. Ganopolski, A. Mangini, C. Kubatzki, K. Roth, and B. Kromer, Nature **438**, 208 (2005).
[10] P. D. Ditlevsen, Geophys. Res. Lett. **26**, 1441 (1999).
[11] P. D. Ditlevsen, M. S. Kristensen, and K. K. Andersen, J. Climate **18**, 2594 (2005).
[12] R. Benzi, G. Parisi, A. Sutera, and A. Vulpiani, Tellus **34**, 10 (1982).
[13] L. Gammaitoni, P. Hänggi, P. Jung, and F. Marchesoni, Rev. Mod. Phys. **70**, 223 (1998).
[14] R. B. Alley, S. Anandakrishnan, and P. Jung, Paleoceanography **16**, 190 (2001).
[15] S. Julier, J. Uhlmann, and H. F. Durrant-Whyte, IEEE Transactions on Automatic Control **45**, 477 (2000).
[16] S. J. Julier and J. K. Uhlmann, Proceedings of the IEEE **92**, 401 (2004).
[17] A. Sitz, U. Schwarz, J. Kurths, and H. U. Voss, Phys. Rev. E **66**, 016210 (2002).
[18] H. U. Voss, J. Timmer, and J. Kurths, Int. J. Bif. Chaos **14**, 1905 (2004).
[19] North Greenland Ice Core Project members, Nature **431**, 147 (2004).
[20] T. Schreiber and A. Schmitz, Phys. Rev. Lett. **77**, 635 (1996).
[21] C. W. Gardiner, *Handbook of Stochastic Methods* (Springer, 2004).
[22] G. Bond, W. Broecker, S. Johnson, J. McManus, L. Labeyrie, J. Jouzel, and G. Bonani, Nature **364**, 143 (1993).
[23] V. Livina, F. Kwasniok, and T. Lenton, submitted.
[24] F. Kwasniok and G. Lohmann, Nonl. Proc. Geophys., submitted.
[25] P. D. Ditlevsen, S. Ditlevsen, and K. K. Andersen, Ann. Glaciol. **35**, 457 (2002).
[26] M. Schulz, A. Paul, and A. Timmermann, Quat. Sci. Rev. **23**, 2219 (2004).